

# Electric Aircraft Propulsion Power System Impedance Modelling Methodology

Dr. Peter Kascak<sup>1</sup>, Dr. Timothy Dever<sup>2</sup>, Ralph H. Jansen<sup>3</sup>  
*NASA Glenn Research Center, Cleveland, Ohio 44135*

**This paper describes techniques to be used to model megawatt Electrified Aircraft Propulsion (MW EAP) components, specifically motor/generators and inverters, DC-DC converters, and long power leads; resulting in impedance-based models which require no information from the component manufacturers. A custom curve fitting method is described, and an example power supply model is fit using measured impedance data. A method called subscale measurement, employing measurement equipment which has much lower power capability than the MW EAP system under test, is described, simulated, and used to generate an impedance transfer function model of a load. Finally, stability analysis using a Nyquist based approach is performed on the combined supply and load system, using the generated models.**

## I. Introduction

NASA is investing in Electrified Aircraft Propulsion (EAP) research, with the goal of improving the fuel efficiency while reducing emissions and noise levels in commercial transport aircraft. The primary EAP configurations which are being evaluated for regional jet and larger aircraft include turboelectric, partially turboelectric, and hybrid electric propulsion systems [1]. To help meet these improvement goals, the NASA Electric Aircraft Testbed (NEAT) has been developed over the past five years, with the goal of providing a testbed to enable end-to-end testing of multiple technologies required in the development of EAP aircraft. NEAT has been designed to be reconfigurable, so the facility can be used to test multiple technologies, and multiple architectures. These technologies include high-power motor/generators and inverters; high-voltage electrical bus architectures; system communication; system fault protection; and system thermal management. One recent configuration was a powertrain test, providing a megawatt-scale dynamometer inside of an altitude chamber, which enabled full-power testing of megawatt-scale components and systems under simulated altitude conditions [2].

A model of the entire megawatt (MW) EAP system is desired, to facilitate study of existing configurations, and provide guidance in the design of future configurations. Goals of these studies include determining systems stability and transient response, providing guidance on power quality, and providing insight into future standards development. Stability of the electrical system is particularly important; previous testing at NEAT has demonstrated, under certain conditions, instability of the DC bus. As the layout of NEAT is intentionally intended to mimic potential MW EAP configurations (i.e. multiple switching power electronics subsystems interconnected with long cables), these early tests clearly demonstrate the hazards of potential power system instability in MW EAP systems in general. Previous instability issues at NEAT were solved via trial and error, a slow and uncertain process; accordingly, direct access to the variables of interest which will allow the understanding of, and enable the control of, power system stability is desired. This is a key goal of this study. Additionally, linkage exists between power system stability, EMI/EMC, and power quality; a further goal would be to provide EMI/EMC compliance in addition to providing improved stability. This will require proper filter design and inclusion, which can add considerable weight; providing stability, EMI/EMC compatibility and power quality with minimum weight filtering components is also desired.

---

<sup>1</sup> Research Engineer, Electrical Power Systems, Diagnostics and Electromagnetics Branch/Power Division.

<sup>2</sup> Research Engineer, Electrical Power Systems, Diagnostics and Electromagnetics Branch/Power Division, AIAA member.

<sup>3</sup> Technical Management, Aeronautics Mission Office, AIAA Member.

The NEAT facility includes 4-quadrant DC power supplies used to represent batteries, and multiple electric machines and associated drive electronics configured to represent electric machines, loads (aircraft propeller/fan), and prime movers (e.g. turbine engines). These systems feature complex interaction between interconnected switching power electronics: DC supplies (sometimes bi-directional); machine/inverter (motor and generator); and DC-DC converters powering loads. Additionally, long cables are employed in the power bus, which must be considered as part of the analysis. It is desired to numerically model this complex system quickly, while retaining the relevant system effects. A brute force approach would be to model every component from the ground up, but this approach is unattractive for numerous reasons. Firstly, this process would be very time consuming, even less attractive when considering that NASA's NEAT facility was designed to be flexible, with frequent hardware changes. Secondly, modeling of this type could require very long simulation times. Thirdly, due to lack of manufacturer information on many of these components, modeling based on component design information is not possible.

Instead, this paper looks at modelling the power system with impedance-based models, requiring no information from the component manufacturers. The models can be generated using data gathered from lab measurements made at the terminals of the device, enabling quick and flexible modeling of components in NASA's NEAT facility. Additionally, these models execute very quickly, because the impedance is a linear system. Another advantage of this modelling technique is that the resulting models can be readily applied to determine the stability and relative stability of the power system. With this type of approach, we are concerned with how components affect the power bus, not the internal workings of these components. Every component is modelled as an ideal voltage source in series with a general impedance, in transfer function form. Schematics of the general supply and load models are shown in Figure 1.

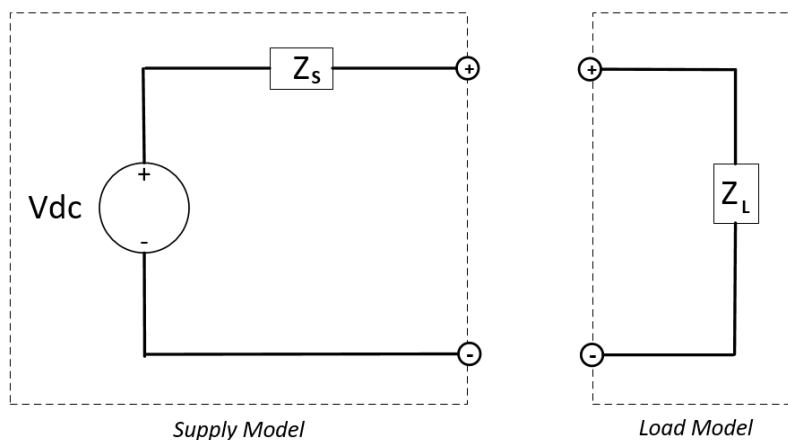


Figure 1. Supply Model and Load Model Configuration

Once developed, the models in Figure 1 can then be used in combination to represent the MW EAP power system. The goal of this research effort is to create this combined model, then test for system stability at test conditions of interest, e.g. at varying powers and speeds, and with machines operating as motors and generators, etc.

This paper is divided into five sections. The first section describes a custom curve fitting method, used to fit transfer function models to measured impedance data. Next, an example fit of measured impedance data for a power supply is demonstrated. Thirdly, a method of taking general impedance measurements, called *subscale measurement*, is described, which injects a sinusoidal test current into the device under test, employing measurement equipment which has much lower power capability than the MW EAP system under test; and a subscale measurement simulation is provided, using the above-generated power supply transfer function. In the fourth section, the subscale measurement simulation approach is used to generate impedance data for a constant power load; and a fit is performed to that data to generate a transfer function model of the load. Finally, stability analysis using a Nyquist based approach is performed on the combined system, using the generated supply and load models.

## II. Transfer Function Curve Fitting

In this section a custom curve fitting method, used to generate transfer functions from measured impedance data for use in modeling and analysis of MW EAP systems, is described.

We wish to convert impedance data generated from lab measurements into transfer functions. Using measured impedance data  $G(j\omega)$ , our preferred model structure would be the ratio of two frequency dependent polynomials,

$$G(j\omega)^* \cong \frac{A_0 + Ap_1 \cdot (j\omega) + A_2 \cdot (j\omega)^2 + \dots + A_n(j\omega)^n}{1 + B_1 \cdot (j\omega) + B_2 \cdot (j\omega)^2 + \dots + B_m \cdot (j\omega)^m} \quad (1)$$

$$= \frac{N(\omega)}{D(\omega)} \quad (2)$$

The error in this proposed fit can be described by

$$\epsilon(\omega) = G(j\omega) - \frac{N(\omega)}{D(\omega)} \quad (3)$$

In order to avoid the complexities of taking partial derivatives of Eq. (3), this error relationship is rearranged to

$$D(\omega) \cdot \epsilon(\omega) = D(\omega) \cdot G(j\omega) - N(\omega). \quad (4)$$

The right side of Eq. (4) can be separated into real and imaginary terms,

$$D(\omega) \cdot \epsilon(\omega) = a(\omega) + ib(\omega), \quad (5)$$

and at any given frequency  $\omega_k$ , the magnitude of this function is

$$|D(\omega_k) \cdot \epsilon(\omega_k)|^2 = a^2(\omega_k) + b^2(\omega_k). \quad (6)$$

By defining Eq. (6) summed over all of the sampling frequencies,

$$E = \sum_{k=0}^m [a^2(\omega_k) + b^2(\omega_k)] \quad (7)$$

the desired coefficients  $A_i$  and  $B_i$  can be calculated by minimizing  $E$ . This is done by taking partial derivatives of  $E$  as a function of each of the desired coefficients, setting these to zero, and rearranging such that a set of equations is calculated which can be expressed in matrix form as

$$M \cdot N = C \quad (8)$$

where  $M$  is a matrix and  $C$  is a vector, all terms of which are calculated from the experimental impedance data; and  $N$  is the vector of the desired fit coefficients, obtained by solving Eq. (8) [3].

An improvement of the above approach is proposed [4] which overcomes some deficiencies through iteration

$$\epsilon_k'' = \frac{\epsilon_k D(j\omega)_L}{D(j\omega)_{L-1}} = \frac{G(j\omega)D(j\omega)_L}{D(j\omega)_{L-1}} - \frac{N(j\omega)_L}{D(j\omega)_{L-1}} \quad (9)$$

where L is the iteration number. Since  $Q(j\omega)$  is not initially known, in the first iteration it is assumed to be one. Eq. (9) is then repeatedly applied until it converges acceptably.

Another improvement upon the above approach was implemented by the authors. To assist in curve fitting, an addition was made to the above implementation, which includes initial guesses of pole and zero locations based on inspection of the measurement data; the measured data is then divided by the assumed transfer function, to improve the numerical fit process.

### III. Curve Fitting Example: Power Supply Model

In this section, an example curve fit using the above-described approach is done, using measured power supply impedance data.

The measured data was taken using a low power capacity Impedance Measurement System (IMS), available to the authors. The IMS is used to inject a test current at a desired frequency through the isolation transformer; then to measure the current and voltage at the input to the test article at the injected current (test) frequency. By repeating this process at a suitable number of test frequencies throughout the range of interest, impedance at those frequencies can be calculated using the measured voltages and currents. The low power impedance measurement was performed on a smaller power supply (40 V, 250 A capability) driving a resistive load over a long set of cables (45' long). The test configuration is shown in Figure 2.

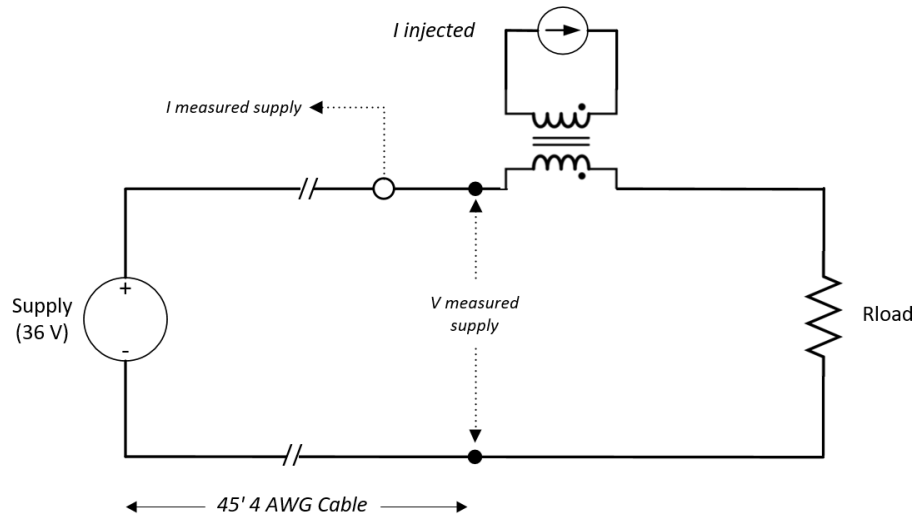


Figure 2. Low Power Capacity Impedance Measurement Configuration

The impedance data captured with the IMS via the low power capacity impedance measurement is shown in Figure 3.

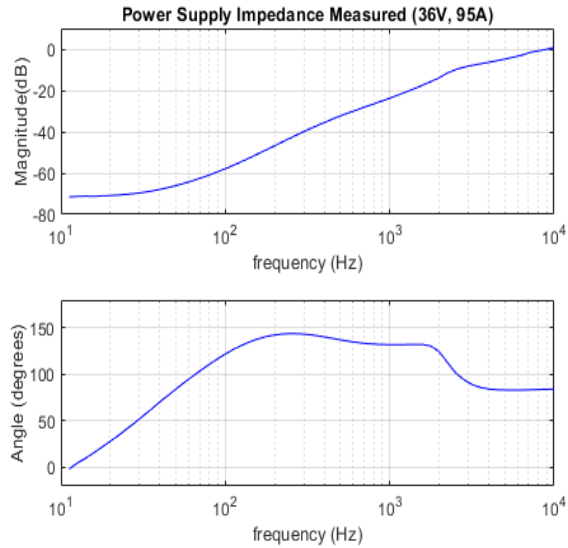


Figure 3. Low Power Capacity Impedance Measurement Data

Next, the measured power supply impedance data was fit to a transfer function model using the process described in the previous section. To improve the model, intuitive guesses of pole and zero location were included in the initial fit: two zeros were assumed at 40 Hz, based on the change in magnitude data slope from 0 to +40 dB/decade; and a pole was assumed at 2400 Hz, based on the decrease to 20 dB/decade near that frequency (see Figure 3). These estimated pole and zero values were then divided out of the measured data, which enabled an improved numerical fit. The measured impedance and the resultant transfer function model are plotted together in Figure 4 Figure 1.

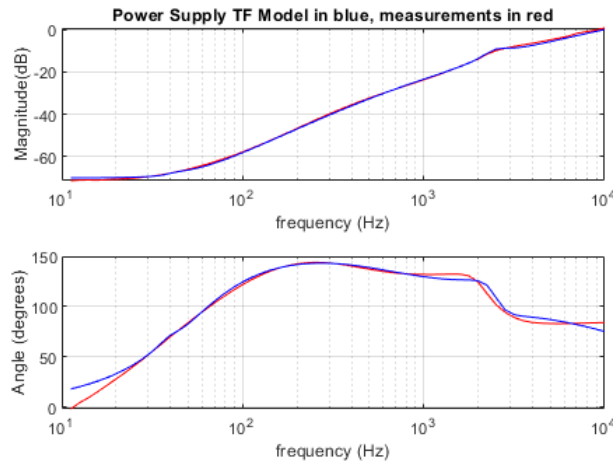


Figure 4. Power Supply Model Fit to Low Power Impedance Measurements

The system poles and zeros for this model are shown in Table 1.

Table 1. Poles and Zeros of Power Supply Model Fit

Model Zeros	Model Poles
$-4.461e3 \pm j1.489e4$	$-1.825e5$
$-1.023e4$	$-2.902e3 \pm j1.541e4$
$-2.483e2 \pm j2.150e2$	$-1.508e4$
$-4.000e1 \pm j2.481e2$	$-3.904e3$
	$-3.851e1 \pm j2.516e2$

A seventh order numerator and denominator transfer function (which includes the initial guess poles and zeros) was selected for the power supply model. A reduced order model (three poles and zeros) was also created which provided a fairly good fit, but did not capture enough detail of the phase variation, which is important in the stability analysis. In order to ensure representation of the relevant detail, the higher order model was used.

As seen in Figure 4, the seventh order fit follows the measured power supply impedance data very well; and so we have achieved our goal of generating a working power supply model, created without the need of any manufacturer-provided information.

#### IV. Subscale Measurement Development and Simulation

In this section, a method of taking general impedance measurements, called *subscale measurement*, is described and implemented in simulation. The power supply model developed in the previous section is used as the system under test; correct detection of this model via subscale measurement also demonstrates the efficacy of the transfer function modeling approach.

Ideally, a measurement such as the one described in Figure 2 would be used to measure MW EAP systems. Unfortunately, our team is presently limited to a lower power IMS unit, which due to isolation transformer limitations has a maximum voltage capability of 600 V, and a maximum current of 100 A. As the MW EAP systems under test will exceed both of these limits, an adaptation of the lower power IMS for use in MW EAP systems was developed. This is called the subscale measurement approach. As access to the lab is restricted as of this writing, this approach was implemented in simulation. A schematic of the subscale measurement simulation is shown in Figure 5.

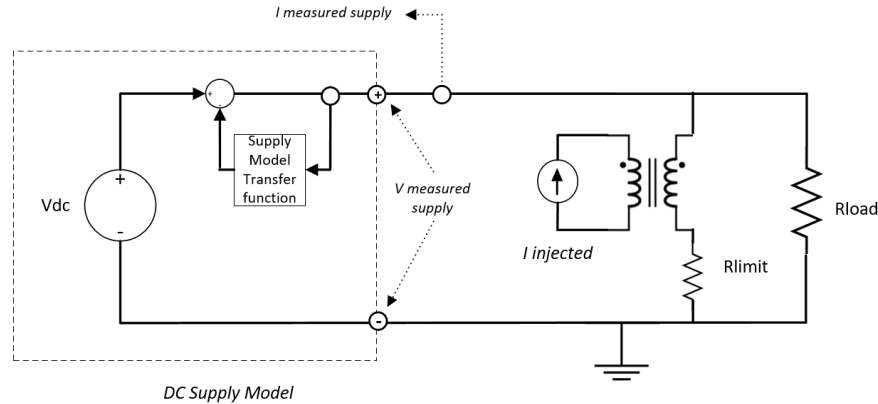


Figure 5. Power Supply Model Subscale Measurement Simulation

In Figure 5, implementation of the IMS is similar to a standard configuration (as seen in Figure 2), in that a current is injected through the isolation transformer, and voltage and current measurements of the system under test are taken. Some notable differences in the subscale measurement approach include the addition of the resistor  $R_{limit}$ , and the addition of post processing analysis. Resistor  $R_{limit}$  is added to enable injection of the current into the test circuit while protecting the isolation transformer;  $R_{limit}$  is sized to be larger than output resistor  $R_{load}$ , limiting the current flowing through the transformer; and the voltage dropped across  $R_{limit}$  ensures that the voltage applied across the transformer is limited as well (if desired, a capacitor could be used in place of  $R_{limit}$  to block any DC current). The measured current and voltage signal post-processing includes band pass filtering centered at the injection frequency, FFTs of the two

signals, and the conversion of the voltage and current data at each point in the test frequency range to an impedance value.

The system under test in this subscale measurement is our DC power supply model. As discussed previously, for this effort source models are implemented using an ideal voltage source and a representative impedance; thus the power supply model is created by combining an ideal DC voltage source and the power supply impedance model. In this case the power supply model used was the transfer function power supply model developed in Section III.

The subscale measurement simulation progresses as follows. A test current frequency is selected from the frequency range of interest, and is injected into the system, while voltages and currents at the test article terminals are measured. The simulation is allowed to run a pre-defined number of cycles to ensure that steady state operation has been achieved; 30 periods in this case. Note that a deliberately low injection current was selected (1 A in this example), in an attempt to ensure that small signal behavior is captured, and that the isolation transformer is kept within its allowed operational range. Once the simulation has completed, the measured and processed voltages and currents for that frequency are stored, and the simulation process is repeated for all frequency points of interest. In this example 120 points across the frequency range were selected, which provided a smooth fit. Once all of these simulations are completed, the voltage and current data is used to generate complex impedance data for the model over the entire frequency range of interest. The results of the subscale simulation are shown in Figure 6.

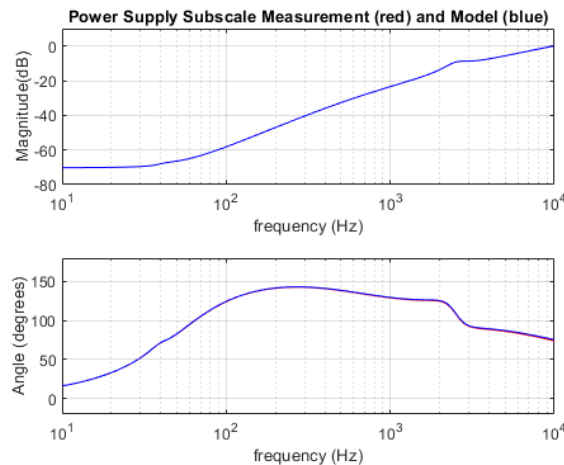


Figure 6. Power Supply Model Subscale Measurement Simulation Results

In Figure 6, the power supply transfer function impedance model is shown in blue, and the extracted subscale measurement is shown in red. Note that the fit is excellent, as it matches the model so well that the fit plot lies almost directly on top of the model plot. Thus the subscale measurement was able to, in simulation, successfully capture the power supply behavior, providing impedance as a function of frequency. Once actual measurements on hardware can be made using the subscale measurement approach, the curve fitting technique will be performed to generate a transfer function model based on the measured impedance data.

This demonstrates a successful simulation of the subscale measurement approach, and also demonstrates a transfer function based impedance model (power supply model) operating correctly in simulation.

## V. Constant Power Load Model

In this section, a subscale measurement simulation is used to generate impedance data for a constant power load (CPL). Next, a transfer function model of the load is generated from this impedance data.

CPLs occur in many ways in modern power systems. Two important implementations in MWEAP include motor drives and DC-DC converters. Consider the case of an inverter and motor driving a propulsor. Over long periods of time the propulsor will be controlled to be at a constant speed; on the time scale of the power system, this will be the case even when the throttle is changed based on the flight profile. The loading this propulsor imparts to the motor drive will also require constant torque, on power system time scales. So the propulsor is spinning at constant speed and loading the motor drive with constant torque, which means the mechanical output power of the motor drive must

be constant power. Because it is assumed that the motor drive is approaching 100 percent efficiency, the input power to the motor drive must also be constant power.

Another common CPL is the DC-DC converter with a regulated output voltage which drives a resistive load. An example is shown in Figure 7.

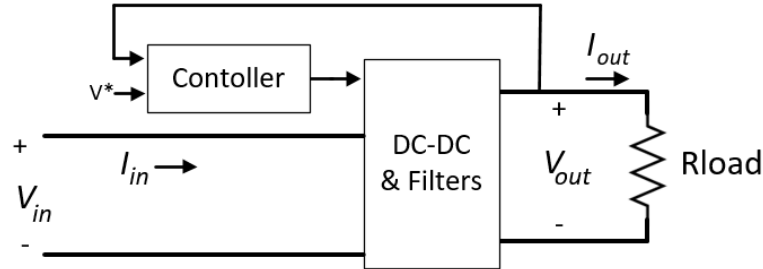


Figure 7. Constant Power Load Schematic

Assuming the converter in Figure 7 has 100% efficiency, the input power is equal to the output power.

$$P_{out} = P_{in} \quad (10)$$

Expanding the expression for input power in terms of voltage and current, this can be rewritten as:

$$P_{out} = I_{in} V_{in} \quad (11)$$

The input current is therefore,

$$I_{in} = \frac{P_{out}}{V_{in}} \quad (12)$$

Here  $I_{in}$  is a function of  $V_{in}$  and  $P_{out}$  is constant. The incremental admittance can be determined by taking the partial derivative of  $I_{in}$  with respect to  $V_{in}$ ,

$$Y_{in} = \frac{\partial I_{in}}{\partial V_{in}} = -\frac{P_{out}}{V_{in}^2} \quad (13)$$

This incremental admittance is real, so it is an incremental conductance. The incremental resistance is the inverse of the incremental conductance,

$$R_{in} = -\frac{V_{in}^2}{P_{out}} \quad (14)$$

Note this input resistance is negative, this negative resistance is what tends to destabilize power systems.

In order to test for stability, it is necessary to model constant power loads. For the rest of this paper a regulated DC-DC converter, as shown in Figure 8, will be used to model a constant power load.

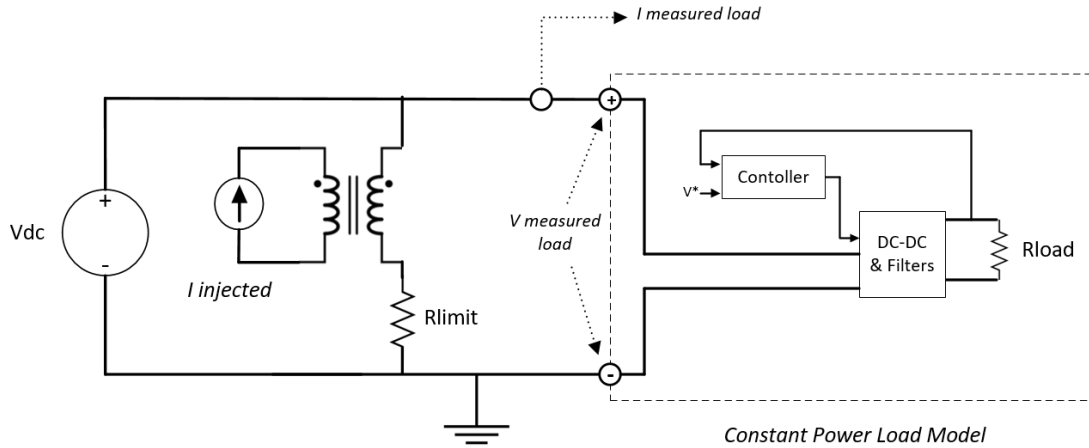


Figure 8. Constant Power Load Subscale Measurement Simulation Schematic

Impedance measurements are made using subscale measurement as shown in Figure 8, similarly to the method used in Figure 5; except this time the input impedance of the constant power load is measured. This simulation includes a DC power supply, a signal injection transformer, and finally the test article (the constant power load). The constant power load includes a DC-DC converter, a controller, and a resistive load. The input and output filters are internal to the DC-DC converter. The controller regulates output voltage by changing the duty cycle of the DC-DC converter; in this case the controller is a PI controller. The results of the simulation are shown in Figure 9.

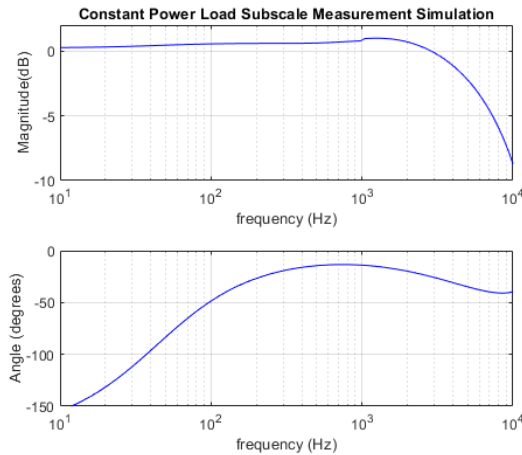


Figure 9. Constant Power Load Subscale Measurement Simulation Results

The previous analysis, provided in Eq. (10) - (14), represents the idealized case of constant power loads. An implicit assumption in this model is that the output is perfectly regulated with infinite bandwidth. Realistically the regulation is only valid for a finite bandwidth. The negative resistance predicted by the ideal case will still appear in the measured impedance at lower frequencies; however, as the frequency increases, the impedance becomes a mixture of the controller and passive components in the circuit. The DC-DC converter is an idealized model and doesn't include switching; however, this model does include the effect of a limited bandwidth controller, in this case a PI controller. Note an LC output filter is also included in the DC-DC converter simulation.

Figure 9 shows a frequency range of 10 Hz to 10 kHz. The impedance does asymptote to 180 degrees at lower frequencies; the 180 degree phase shift means it is acting as a negative resistance at those frequencies, as expected. Also the magnitude at low frequency can be calculated using Eq. (14); here this equation can be expressed in terms of magnitude dB as:

$$|R_{in}|_{db} = 20 \log\left(\frac{V_{in}^2}{P_{out}}\right) \quad (15)$$

In this case the input voltage is 350 V and the output power is about 117 kW, which implies that the magnitude is about 0.4 dB. Another way to calculate this can be seen by substituting the following two equations into (15):

$$P_{out} = \frac{V_{out}^2}{R_{Load}} \quad (16)$$

$$V_{in} = \frac{1}{D} V_{out} \quad (17)$$

which yields [5]

$$|R_{in}|_{db} = 20 \log\left(\frac{R_{Load}}{D^2}\right) \quad (18)$$

Here  $D$  is the duty cycle, which in this case is 0.5, and  $R_{Load}$  is the output resistive load, which is about 260 m $\Omega$ . Evaluating this, it is again seen that the input magnitude is about 0.4 dB; as expected at low frequency, Figure 9 reflects this impedance magnitude. Figure 9 also shows the magnitude and phase of the impedance diverging from the ideal case as frequency increases; this is expected due to the finite bandwidth of the controller. It is seen that the controller loses the ability to regulate the output voltage at higher frequencies, causing the impedance to eventually be dominated by the passive components in the circuit.

Next, we curve fit this subscale measurement simulation output data to a transfer function. Using the above-described transfer function curve fitting algorithm, a good fit was obtained with a 3<sup>rd</sup> order numerator and denominator. Figure 10 shows the fit; note the very close agreement in magnitude and phase. The poles and zeros of the CPL transfer function model are listed in Table 2.

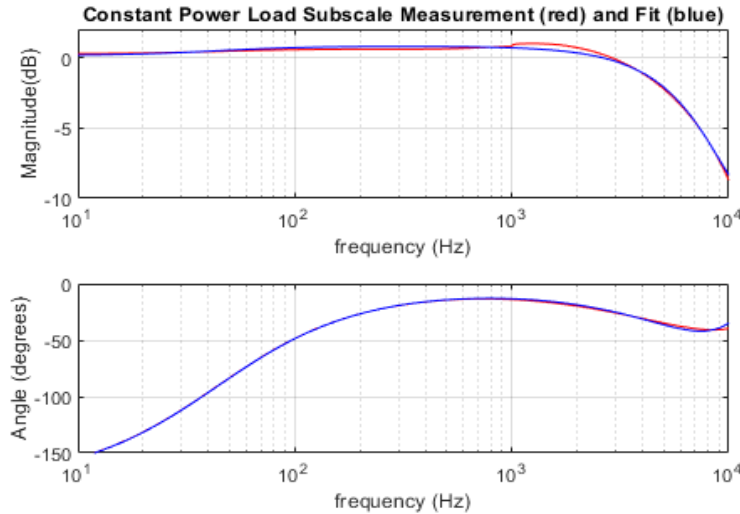


Figure 10. Constant Power Load Model Fit to Subscale Measurement Simulation Results

Table 2. Poles and Zeros of Constant Power Load Model Fit

Model Zeros	Model Poles
$-3.111e+4 \pm j7.115e+4$	$-5.327e+4 \pm j1.9163e+4$
$-2.684e+2$	$2.895e+2$

We have now completed the subscale measurement simulation of a CPL, and developed a representative impedance-based transfer function model for the CPL.

## VI. System Stability Analysis

In this section, stability analysis using a Nyquist based approach is performed on the combined power supply and load system, operating at several output power levels, using the generated transfer function based impedance models. Figure 11 shows the general case of a power supply driving a load, where a voltage source is included in the load.

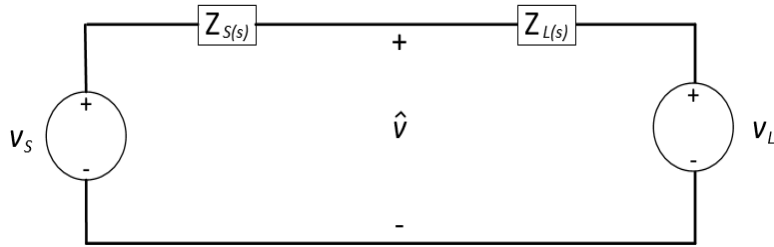


Figure 11. Impedance Model, Source and Load

For this analysis it is assumed that there is no voltage source in the load, thus  $v_L = 0$ . Implementing the supply and load models developed in the above sections, the schematic of the combined system is shown in Figure 12.

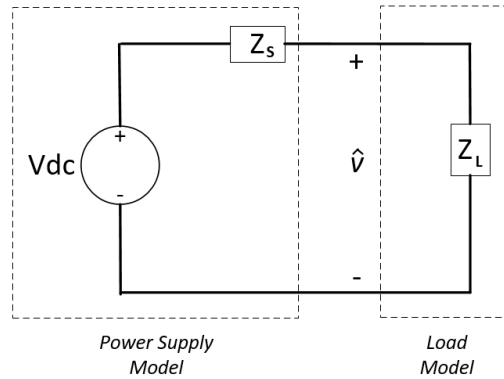


Figure 12. Combined Model Stability Test Configuration

The voltage across the load is described as

$$\hat{v}(s) = \frac{Z_L}{Z_S + Z_L} v_{dc} \quad (19)$$

Dividing the numerator and denominator by  $Z_L$  yields the following:

$$\hat{v}(s) = \frac{1}{1 + \frac{Z_S}{Z_L}} \quad (20)$$

Note this is the closed loop transfer function. Control theory has shown that the closed loop transfer function can be expressed as [6]

$$M(s) = \frac{G(s)}{1 + H(s)G(s)} \quad (21)$$

where the minor loop gain can be identified as

$$T(s) = H(s)G(s) \quad (22)$$

In this case we can describe the minor loop gain in terms of impedances

$$T(s) = \frac{Z_S}{Z_L} \quad (23)$$

and  $1 + T(s)$  must not have any roots in the right half-plane (RHP) to ensure system stability. This is equivalent to stating that  $T(s)$  must satisfy the Nyquist stability criterion [5].

Accordingly, in order to guarantee stability of this system, the number of counterclockwise encirclements of the point  $-1 + j0$  in the Nyquist plot of  $T(s)$  must equal the number of poles of  $T(s)$  in the RHP [6]. To perform this analysis, first the number of poles in the RHP is determined. Table 1 shows that the power supply output impedance has no poles in the RHP. Because  $T(s)$  is defined as the power supply impedance divided by the load impedance, the presence of poles in the RHP of the load impedance is not significant; instead the number of zeros in the RHP of the load impedance is important. Table 2 shows that the constant power load has no zeros in the RHP. Therefore,  $T(s)$  has no poles in the RHP, and stability will be achieved with no encirclements of  $-1$ . The Bode plots of the power supply and load models are shown in Figure 13, and the Nyquist stability plot for the combined system (called the *base load case*) is shown in Figure 14. Note that the Nyquist plot features logarithmic amplitudes, ranging from  $-60$  dB to  $+60$  dB, with  $0$  dB at the center solid circle [7].

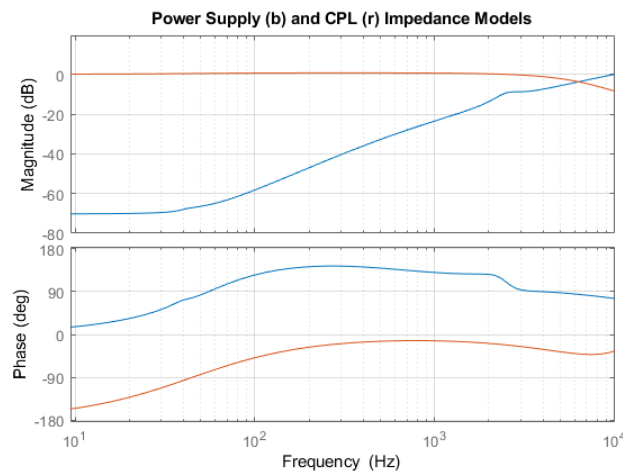


Figure 13. Bode Plots, Source and Load Impedance

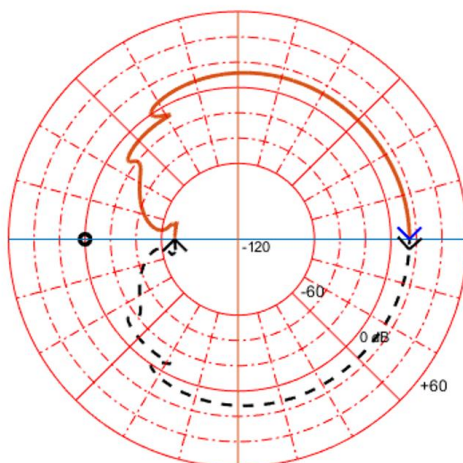


Figure 14. Nyquist Stability Plot, Base Load Case

In Figure 14, we see that the Nyquist curve for the combined system doesn't encircle -1 in the base load case. Since  $T(s)$  has no poles in the RHP, the Nyquist stability criterion is met, and this power source and load combination is stable. However, in addition to absolute stability, it is advantageous to also meet a relative stability criterion. Meeting a certain gain and phase margin has benefits; it will allow the system to remain stable if the system changes slightly over time, and will account for potential modelling errors, etc. In addition, relative stability margins will help guarantee a reasonable power system response; for example, to ensure adequate damping for all system disturbances. A common approach to power system relative stability is called GMPM (Gain Margin Phase Margin) [8]. A standard power system specification is to have a gain margin of 6 dB and a phase margin of 60 degrees. This defines a forbidden region, shown in blue and applied to the base load case, shown in Figure 15.

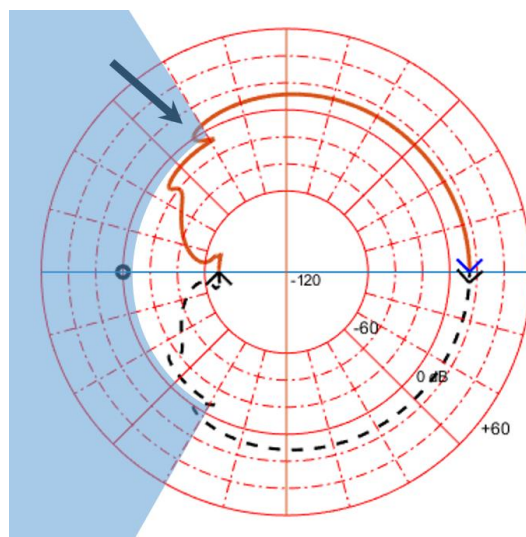


Figure 15. Nyquist Stability Plot with GMPM Forbidden Region, Base Load Case

In Figure 15, we see that plot of the base load case enters the forbidden region, and thus violates the described GMPM criteria (6 dB and 60 degrees) because the Nyquist plot exceeds 0 dB within the 60 degree limit (marked by arrow). Therefore, some modification would be required in order for this system to meet the stated relative stability criteria under these operating conditions.

It is worth noting the impact of output power level on the stability of this system. If the power consumed by the load is reduced, the impedance of the load is increased, per Eq. (15); thus reduction of the load power will modify the system minor loop gain  $T(s)$ . As an example, the Nyquist plot of this source-load model with the CPL output power reduced by a factor of 10 is shown in Figure 16.

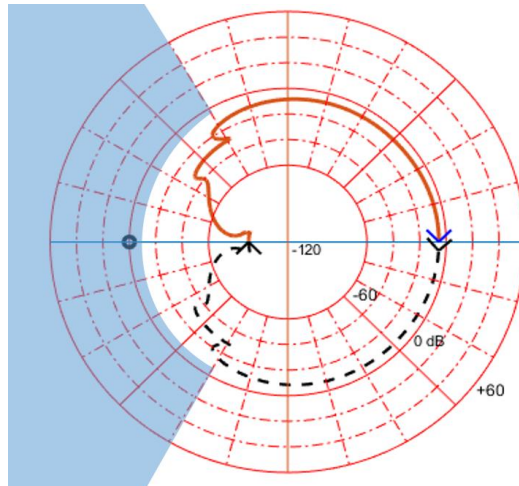


Figure 16. Nyquist Stability Plot, Reduced Power Load

In Figure 16, we see that the GMPM criteria of 6 dB and 60 degrees is clearly met in the reduced load power case.

As intended, we have provided a stability analysis on the combined power supply and load system operating at several power levels, using the generated transfer function impedance models, implementing a Nyquist based approach.

## VII. Conclusion

This paper examines issues of modelling MW EAP systems in the context of NASA's NEAT facility. One approach to modelling these systems would be to model hardware on a one to one basis with real hardware. For example, with the same switching converters, at the same switching frequencies, with the same controllers, etc. This is certainly a good approach for certain types of modelling studies, where this type of detail is required. However, there are several downfalls to such approaches, especially when studying the system as a whole, instead of small parts. One major downfall is the large difference in the timescales of various models, e.g. between fundamental electrical frequencies, and those required to represent mechanical systems dynamics, and aircraft operations timescales. Modelling the power system including all these effects would require very long simulation times, limiting the usefulness of such a simulation. Another major drawback of such an approach is the time required to develop such simulations. Additionally, NASA's NEAT facility is very flexible and hardware can be changed frequently. This involves both COT's hardware and proprietary hardware, where it can be very difficult to obtain the necessary detailed information; even if this information were readily available, the development time of these types of models is restrictive.

This paper presents impedance modelling, which has many advantages over other modelling methods. A major advantage of this approach is that impedance modelling doesn't require detailed knowledge of the internal workings of power components. The models can be made quickly with lab measurements made at the terminals of the device. This quick modelling capability enables the flexibility needed for NASA's NEAT facility. Additionally, these models execute very quickly, because the impedance is a linear system. Another advantage of this modelling technique is that the resulting models can be readily applied to determine the stability and relative stability of the power system.

First, this paper presents a method to curve fit experimental impedance data, amplitude and phase, to a transfer function, i.e. a ratio of complex polynomials. This curve fitting algorithm enables the automatic generation of models very quickly.

Secondly, this paper demonstrates a power supply model development, using impedance data measured on a commercial power supply with long leads. This impedance data was curve fit to a transfer function, and a model of the power supply was then created with an ideal voltage source in series with the impedance transfer function.

Next, an experimental technique is explained to obtain the output impedance of a power supply, using a commercially available impedance test device which was designed for low power systems. Called subscale measurement, this method demonstrates how this low power test device can be used on higher power systems without exceeding the power limitations of the impedance testing device. This method was carried out in simulation, and the results match the impedance used in the power supply model.

This paper then describes constant power load modeling. Constant power loads appear often in power systems, and are critical to understand, as they tend to be destabilizing. It is shown how constant power loads tend to create negative incremental resistances for certain frequency ranges. This paper uses a DC-DC converter with a regulated output as the constant power load. The subscale measurement testing method which was demonstrated on the power supply was then applied to the constant power load, and the curve fitting algorithm was used on the resultant impedance measurements to develop an impedance-based model of the constant power load.

Finally, this paper shows how the power supply and constant power load models can be combined, and used to determine the stability of the entire power system. It is shown that Nyquist stability plots can be created to determine stability. In addition, it is shown that relative stability can be determined using the same Nyquist plots.

### Acknowledgments

This work is sponsored by the NASA Advanced Air Transportation Technologies Project/Power and Propulsion Subproject managed by Amy Jankovsky. The work is performed at NASA Glenn Research Center.

### References

- [1] Jansen, R., C. Bowman, A. Jankovsky, R. Dyson and J. Felder. "Overview of NASA Electrified Aircraft Propulsion Research for Large Subsonic Transports." *2017 AIAA Propulsion and Energy Forum*, 10-12 July 2017, Atlanta, Georgia, USA.
- [2] Haglage, J., Brown, T. "NASA Electric Aircraft Testbed (NEAT) Reconfiguration to Enable Altitude Testing of Megawatt-Scale Electric Machines," *2020 AIAA/IEEE Electric Aircraft Technologies Symposium (EATS)*, 2020, pp. 1-13.
- [3] Levy, E. "Complex-curve fitting," in *IRE transactions on automatic control*, Volume AC-4, pp. 37-44, 1959.
- [4] Sanathanan, C. and Koerner, J. "Transfer function synthesis as a ratio of two complex polynomials," *IEEE Transactions on Automatic Control*, Volume 8, Issue 1, pp. 56-58, January 1963.
- [5] Middlebrook, R.D., "Input Filter Considerations in Design and Application of Switching Regulators," *IEEE IAS Annual Meeting*, 1976.
- [6] Dorf, R. C., and Bishop, R. H., *Modern Control Theory*, 13<sup>th</sup> edition, New York, NY, USA, Pearson Education Limited, 2017.
- [7] Trond Andresen (2021). Nyquist plot with logarithmic amplitudes (<https://www.mathworks.com/matlabcentral/fileexchange/7444-nyquist-plot-with-logarithmic-amplitudes>), MATLAB Central File Exchange. Retrieved May 13, 2021.
- [8] Wildrick, C. M.; Lee, F. C.; Cho, B. H.; Choi, B., "A method of defining the load impedance specification for a stable distributed power system," *IEEE Transactions on Power Electronics*, vol. 10, no. 3, pp. 280-285, May 1995.